

# *Climatology of banded precipitation over the contiguous United States*

Article

Published Version

Creative Commons: Attribution 4.0 (CC-BY)

Open Access

Fairman, J. G., Schultz, D. M., Kirshbaum, D. J., Gray, S. L. ORCID: <https://orcid.org/0000-0001-8658-362X> and Barrett, A. I. (2016) Climatology of banded precipitation over the contiguous United States. *Monthly Weather Review*, 144 (12). pp. 4553-4568. ISSN 0027-0644 doi: 10.1175/MWR-D-16-0015.1 Available at <https://centaur.reading.ac.uk/67366/>

It is advisable to refer to the publisher's version if you intend to cite from the work. See [Guidance on citing](#).

Published version at: <http://dx.doi.org/10.1175/MWR-D-16-0015.1>

To link to this article DOI: <http://dx.doi.org/10.1175/MWR-D-16-0015.1>

Publisher: American Meteorological Society

All outputs in CentAUR are protected by Intellectual Property Rights law, including copyright law. Copyright and IPR is retained by the creators or other copyright holders. Terms and conditions for use of this material are defined in the [End User Agreement](#).

[www.reading.ac.uk/centaur](http://www.reading.ac.uk/centaur)

**CentAUR**

Central Archive at the University of Reading

Reading's research outputs online

# Climatology of Banded Precipitation over the Contiguous United States

JONATHAN G. FAIRMAN JR. AND DAVID M. SCHULTZ

*Centre for Atmospheric Science, School of Earth, Atmospheric and Environmental Sciences, University of Manchester, Manchester, United Kingdom*

DANIEL J. KIRSHBAUM

*Department of Atmospheric and Oceanic Sciences, McGill University, Montreal, Quebec, Canada*

SUZANNE L. GRAY AND ANDREW I. BARRETT

*Department of Meteorology, University of Reading, Reading, United Kingdom*

(Manuscript received 7 January 2016, in final form 4 July 2016)


## ABSTRACT

A climatology of banded-precipitation features over the contiguous United States from 2003 to 2014 is constructed. A band is defined as a precipitation feature with a major axis of 100 km or greater and a ratio of major axis length to minor axis length (hereafter, aspect ratio) of 3:1 or greater. By applying an automated feature-based detection algorithm to composite radar imagery, a database of 48 916 844 precipitation features is created, of which 7 213 505 (14.8%) are bands. This algorithm produces the first climatology of precipitation bands over the contiguous United States. Banded-precipitation occurrence is broadly similar to total precipitation occurrence, with a maximum of 175 h of banded precipitation annually over the Ohio River valley. In the warm season, there is a strong diurnal signature associated with convective storm development for both the precipitation feature area and total area covered by precipitation, but little diurnal signature in aspect ratio. Strong west–east gradients in both precipitation occurrence and banded-precipitation occurrence exist, as areas west of the Rockies receive less frequent precipitation, which is much less likely to be banded. East of the Rockies, precipitation features are banded 30% of the time, versus 10%–15% west of the Rockies. Areas downwind of the Great Lakes show prominent late autumn and winter maxima in banded precipitation associated with lake-effect snowbands. Local maxima of banded-precipitation percentage occur in the Dakotas and east of the Colorado Rockies during winter. Although banded-precipitation features compose only 14.8% of all precipitation features, they contribute 21.9% of the annual precipitation occurrence over the contiguous United States.

## 1. Introduction

The organization of clouds and precipitation into linear or quasi-linear bands is a striking characteristic of the atmosphere. These bands occur on various scales, ranging from embedded bands in extratropical cyclones that are hundreds or thousands of kilometers in length

(e.g., Houze et al. 1976; Hobbs 1978; Houze and Hobbs 1982; Parsons and Hobbs 1983; Novak et al. 2004, 2006, 2009; Norris et al. 2014; Rauber et al. 2014), to bands hundreds of kilometers long related to cold-air outbreaks over or downwind of water bodies (e.g., Niziol et al. 1995; Miner and Fritsch 1997; Norris et al. 2013) or over land (e.g., Schultz et al. 2004), to mesoscale bands over or located downstream of orography that are hundreds to tens of kilometers long (e.g., Snook 1992; Davis 1997; Kirshbaum and Durran 2005a,b; Kirshbaum et al. 2007a,b; Schultz and Knox 2007; Andretta and Geerts 2010; Schumacher et al.

 Denotes Open Access content.

*Corresponding author address:* Dr. Jonathan G. Fairman, Centre for Atmospheric Science, School of Earth, Atmospheric and Environmental Sciences, University of Manchester, Simon Building, Oxford Road, Manchester M13 9PL, United Kingdom.  
E-mail: jonathan.fairman@manchester.ac.uk



This article is licensed under a [Creative Commons Attribution 4.0 license](https://creativecommons.org/licenses/by/4.0/).

2010, 2015; Andretta 2014; Barrett et al. 2015, 2016). These banded-precipitation events occur in various locations and under different synoptic regimes and environmental conditions, which, combined with the broad range of band geometries, can make it difficult to examine their properties and determine their occurrence in a systematic way.

Many previous investigations of banded precipitation have relied on manual methods to detect the presence of precipitation bands. Regional investigations of different types of banded precipitation have been conducted over the Pacific Northwest (e.g., Houze et al. 1976; Mass 1981; Kirshbaum and Durran 2005a,b; Kirshbaum et al. 2007a,b), the northeastern United States (e.g., Novak et al. 2004, 2006, 2009), the English Channel and Irish Sea (Norris et al. 2013), the Cevennes area of France (Miniscloux et al. 2001; Cosma et al. 2002; Anquetin et al. 2003; Godart et al. 2009), and northern Japan (Yamada et al. 2012). Because these studies identified bands based on intensity thresholds that may be specific to the particular process and/or region of interest, a different method is needed to conduct a more uniform climatology over a large region like the contiguous United States.

Several automated climatologies of precipitation features have used data from the Tropical Rainfall Measuring Mission (TRMM). Nesbitt et al. (2000) described a method of measuring real-time precipitation features from TRMM, forming the basis of a global precipitation database that has been updated for the past several years as the University of Utah TRMM precipitation-feature database. This precipitation-feature database has been used to determine storm morphology and rainfall characteristics (Nesbitt et al. 2006) and to examine mesoscale banded features associated with the Madden–Julian oscillation (Xu et al. 2015). Liu et al. (2008) extended this database to include information about feature size, determining population-based estimates for mesoscale features and exemplifying how to form and analyze a feature-based dataset. However, the TRMM precipitation radar is limited to areas between 35°S and 35°N, with coverage at a specific point only once every few hours. Therefore, short-lived precipitation features in the tropics, and all precipitation in the midlatitudes (including most of the mesoscale banded-precipitation features within the contiguous United States), are not captured. In addition to the above-mentioned TRMM studies, Smalley and L'Ecuyer (2015) presented a 4-yr global climatology of the precipitation features using the W-band radar on board *CloudSat*. They described annual patterns of the shape factor and scale length of clouds on a 2° × 2° latitude–longitude grid to determine the annual likelihood of precipitation.

When regions of banded precipitation are fixed over a certain point or trail downwind from a given point for a

long period of time, they can produce extreme rainfall totals. Given their narrow width, such bands may not be captured by rain gauges, yet may have a large influence on the meteorology and climatology of a particular region. Knowledge of the spatial pattern of banded-precipitation occurrence from radar or satellite data can help us to understand the physical reasons behind the banding and provide a dataset for verifying model forecasts to see if the modeled features resemble those that are observed. These issues motivate the present study.

This study is the first automated climatology of banded precipitation across the contiguous United States. The goal is to determine the regions where banded precipitation preferentially occurs and to characterize the banded precipitation in these regions by occurrence, contribution to total precipitation, and annual and diurnal cycles. Through this climatology, we use the analysis to infer some dominant physical mechanisms of band formation in different regions. The identification of banded features is accomplished through an automated feature-based detection scheme from imagery of U.S. radar mosaics to detect banded-precipitation features.

The radar composite used in this study and the feature-based banded-precipitation detection algorithm are presented in section 2, with the precipitation feature climatology discussed in section 3. The diurnal and annual cycles of precipitation features and bands are analyzed in section 4. Spatial analysis of the occurrence of precipitation at different intensities and banded precipitation is examined in section 5. The annual cycle of banded precipitation is discussed in section 6, and regions identified as local maxima of banded features are discussed in section 7. Section 8 presents a discussion, and section 9 contains the conclusions.

## 2. Data and methods

To identify banded precipitation over the United States during 2003–14, we use the Iowa Environmental Mesonet NEXRAD mosaic ([https://mesonet.agron.iastate.edu/docs/nexrad\\_composites/](https://mesonet.agron.iastate.edu/docs/nexrad_composites/)). The mosaic (an example is shown in Fig. 1a) is available every 5 min from 1995 to the present and has a 1-km horizontal grid spacing. The mosaic uses level-III base radar reflectivity factors (lowest elevation angle of 0.5°) from about 130 WSR-88D sites across the contiguous United States to produce a PNG-formatted image that is 6000 × 2600 pixels at four-bit resolution (equating to a 5-dBZ interval for each different color in the image). Data are included in the cool season (November–March) when the radars are in both clear-air mode and precipitation mode, and data are included in the warm season (April–October) when the radars are in precipitation mode only. Although clutter-removal techniques are used on the level-III radar



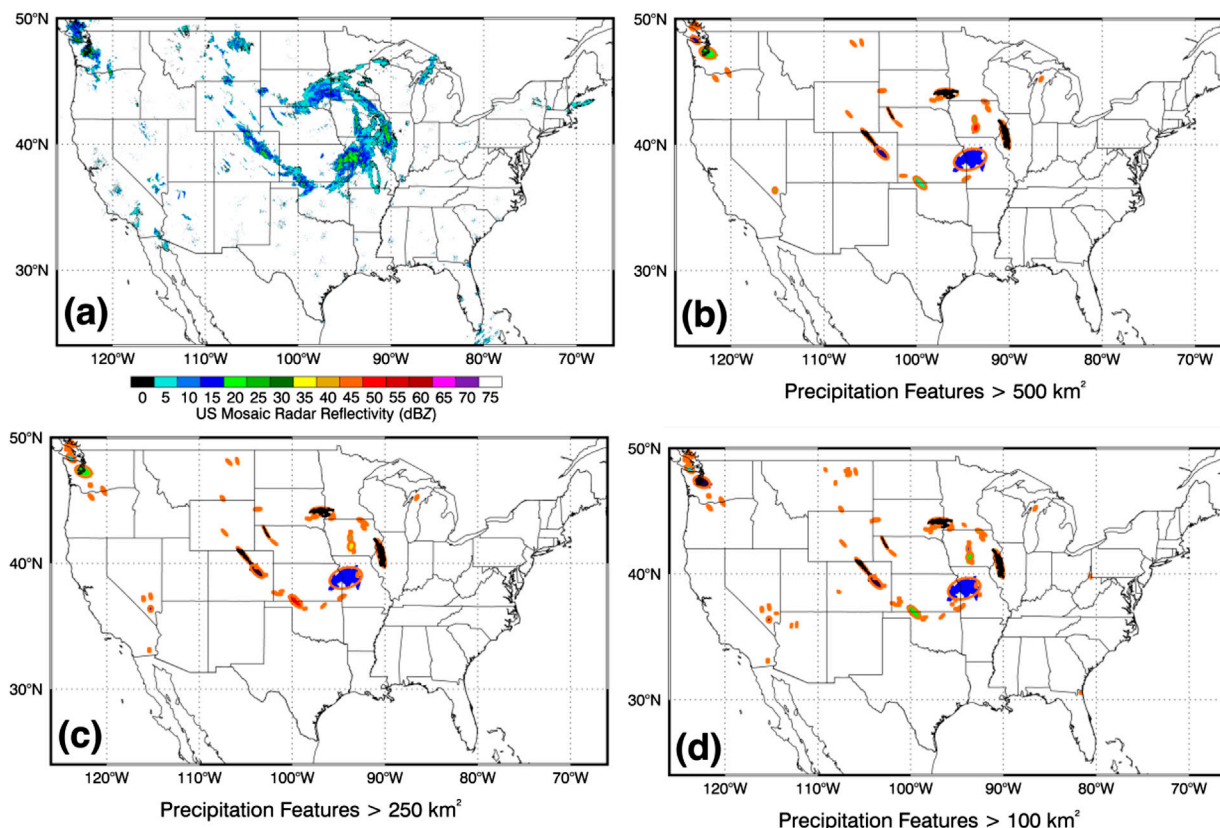


FIG. 1. (a) Iowa Environmental Mesonet U.S. radar composite for 2300 UTC 16 Feb 2007. (b) Detected precipitation features exceeding  $500 \text{ km}^2$  with fitted ellipses. Banded-precipitation features are in black. (c) Detected precipitation features exceeding  $250 \text{ km}^2$ . (d) Detected precipitation features exceeding  $100 \text{ km}^2$ .

data, clutter is still present in the final product (e.g., the northeastern United States and Southern California in Fig. 1a). Although the radar coverage nominally spans across all of the contiguous United States, several areas in the western United States have no radar coverage (Westrick et al. 1999; Maddox et al. 2002).

In this study, a mask of precipitating systems was created, identifying “precipitating” reflectivities greater than or equal to 20 dBZ (the lowest green in Fig. 1a). This precipitation mask was used to determine individual contiguous *precipitation features*, where contiguity is defined as a connection in any direction to another precipitating point. For this study, we consider precipitation features with areas greater than or equal to  $500 \text{ km}^2$  (Fig. 1b), which compose a set of 48 916 844 features over the 12 yr of analysis. A mass–density method of ellipse fitting of the precipitation features was used to determine major and minor axes for each precipitation feature (Fig. 1b), as has been used in other precipitation feature studies (e.g., Nesbitt et al. 2006; Xu et al. 2015). Because detection of features relies on the contiguity of areas where reflectivity is equal to or exceeds 20 dBZ, gaps in

radar coverage may disrupt bands in areas such as in the western United States.

Within this article, a *banded-precipitation feature* (or *band*) is defined as a precipitation feature with a major axis of 100 km or greater and a ratio of major axis length to minor axis length (hereafter, aspect ratio) of 3:1 or greater. Bands are colored black in Figs. 1b–d. These criteria for precipitation bands are similar to those used by Novak et al. (2004) to determine embedded bands within extratropical cyclones, following similar characterizations of bands from Houze et al. (1976). Each feature from the 5-min precipitation mask was classified as either banded or nonbanded. The advantage of this approach is its efficiency (each day consisting of 288 images is processed in only a few minutes), allowing for rapid analysis over the 12 yr of data. Out of the 48 916 844 contiguous precipitation features that equal or exceed  $500 \text{ km}^2$  in area, 7 213 556 (14.8%) are considered banded by these criteria.

To test the sensitivity of the algorithm to detect precipitation bands to the minimum feature size, different minimum thresholds in area were considered (i.e.,  $250 \text{ km}^2$

in Fig. 1c; 100 km<sup>2</sup> in Fig. 1d). These smaller thresholds added a substantial computational expense, as they increased the total number of precipitation features detected by up to an order of magnitude. A sensitivity analysis was performed for different feature minimum areas of 400, 500, and 600 km<sup>2</sup> and for different minimum contiguous reflectivity values of 15, 20, and 25 dBZ. Minima of 600 and 500 km<sup>2</sup> detect 99.2% and 99.7%, respectively, of banded features detected by a minimum feature area of 400 km<sup>2</sup>. A minimum feature area of 400 km<sup>2</sup> increases the total (banded and nonbanded) features detected by over 20% compared to a minimum feature area of 500 km<sup>2</sup>, adding significant computational expense. Reducing the minimum reflectivity threshold to 15 dBZ for all three different feature sizes increases the detected features surrounding the Great Lakes and increases the hours of detected banded precipitation, but the percentage of banded-precipitation occurrence remains nearly constant (22.5% for a minimum reflectivity of 15 dBZ compared to 21.9% for 20 dBZ and 19.8% for 25 dBZ). Although the number of identified features change as these two thresholds varied, the spatial distribution of the bands did not change much (not shown). Because the goal of this study is to identify precipitation bands with major axes exceeding 100 km efficiently, the 500-km<sup>2</sup> minimum detected feature area and 20-dBZ minimum contiguous threshold for reflectivity were chosen.

This method can detect different types of banded features irrespective of their origin, such as the stationary snowbands over Colorado on 16 February 2007 (Schumacher et al. 2010; Figs. 2a,b), the eastern United States derecho of 13 June 2013 (Schmit et al. 2015; Figs. 2c,d), and lake-effect snowbands to the east of Lake Ontario in New York on 23 November 2013 (Figs. 2e,f). These results show that, despite the imposed size threshold, some very narrow precipitation bands are detected by this method.

Maps of the banded-precipitation features detected from 5-min feature data over the 12 yr of study are used as a basis for regional analysis. Two different measures of occurrence are considered. The first is the occurrence of banded precipitation (hereafter, banded occurrence), defined as the number of hours per year when banded precipitation occurs at each grid point. The second is the percentage of time that precipitation is banded (hereafter, banded percentage), calculated as 100 multiplied by the ratio of the banded-precipitation feature occurrence to the occurrence of any precipitation. Precipitation occurrence is defined as all radar reflectivity values of 20 dBZ or greater, even if the precipitation feature has an area of less than 500 km<sup>2</sup>, which reduces the sensitivity of the banded percentage

to the minimum detected feature size. The banded occurrence and banded percentage are complementary metrics because they indicate both the presence of the bands and their relative contributions to the precipitation climatology.

### 3. Distribution of precipitation feature shape and area

Three properties characterize banded precipitation in our feature-based analysis: area of a precipitating system, length of the major axis, and aspect ratio. The distribution of precipitation-feature area for the full dataset of 48 916 844 features and the 7 213 556 banded-precipitation features has a lognormal-type distribution, with 90% of precipitation features sized between 500 and 10 000 km<sup>2</sup> and 95% of precipitation features sized less than 20 000 km<sup>2</sup> (Figs. 3a,b). Considering only banded-precipitation features, the cumulative distribution function of the feature area has a similar shape to all features, but the distribution is shifted to the right, with only 80% of banded-precipitation features being smaller than 10 000 km<sup>2</sup> (Figs. 3a,b). Focusing on the large end of the feature-size spectrum, only 1% of all precipitation features are larger than 100 000 km<sup>2</sup> (about the size of Indiana), whereas the largest banded-precipitation features are only around 50 000 km<sup>2</sup>, or about the size of Vermont and New Hampshire combined (Fig. 3b). Although the mean precipitation-feature area is 5596 km<sup>2</sup>, the median feature area is only 1183 km<sup>2</sup>, compared to the mean banded precipitation-feature area of 11 857 km<sup>2</sup> and median banded precipitation-feature area of 2895 km<sup>2</sup>. Even without specifying the minimum axis length for determining a banded feature, the mean area for a precipitation feature with a 3:1 aspect ratio is 6435 km<sup>2</sup>, with a median area of 1233 km<sup>2</sup>, demonstrating that banded-precipitation features are generally larger than precipitation features overall. Even though the banded features are a subset of the total features, the banded features have significantly different means as determined by a Student's *t* test and significantly different variances as determined by the *F* test, both at greater than the 99.9% level.

The distribution of the mean major-axis length is roughly similar in shape to the distribution of the precipitation-feature area (cf. Figs. 3a,c); 33% of all precipitation features have major axes longer than 100 km, 10% have major axes longer than 200 km, and 5% have major axes longer than 400 km. The mean axis length for precipitation features is 117 km, with a median axis length of 75.2 km. Because a minimum major-axis length of 100 km defines banded-precipitation

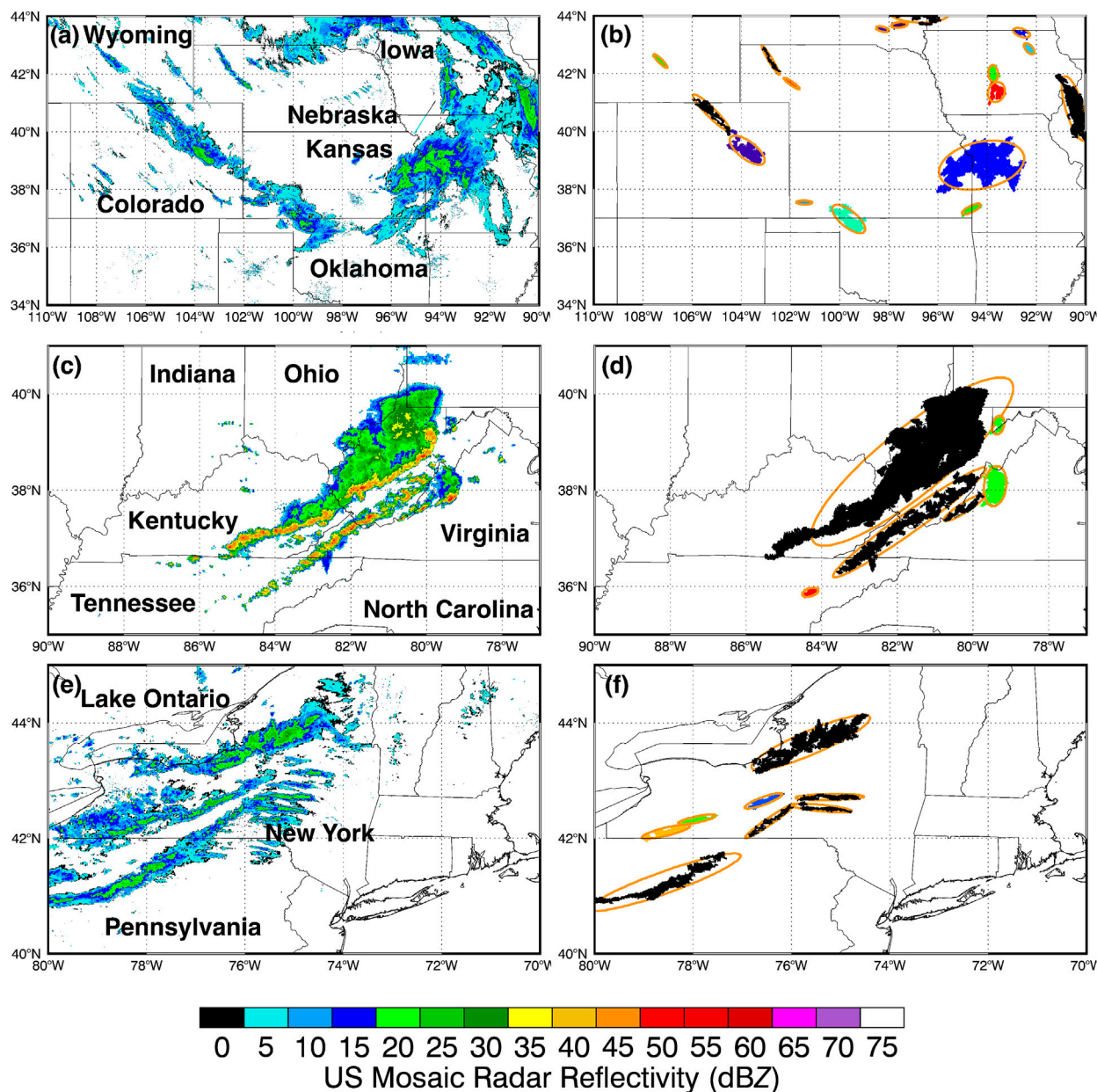


FIG. 2. Example radar composites and detected precipitation features for different types of banded-precipitation events. Banded-precipitation features are colored black while nonbanded features are colored. (a) Radar composite for a banded-precipitation event to the east of the Colorado Rockies at 2300 UTC 16 Feb 2007, as per Fig. 1. (b) Detected features from Fig. 1a. (c) Radar composite over the Ohio Valley at 1700 UTC 13 Jun 2013 depicting a derecho event. (d) Detected precipitation features for (c). (e) Radar composite over NY showing a lake-effect snow event at 1900 UTC 23 Nov 2013. (f) Detected precipitation features shown in (e).

features, their cumulative distribution is quite different than that for all precipitation features. Although 75% of banded features have major axes shorter than 200 km, only 5% of banded-precipitation features have a major axis longer than 600 km. The mean major-axis length for a banded-precipitation feature is 241 km, and the median is 159 km. The distribution of aspect

ratio for precipitation features is different from the distributions of area and major-axis length, with a shallower slope for aspect ratios of 1.5–3.0 (Fig. 3d) compared to the middle range of the cumulative distribution for other feature characteristics. The mean aspect ratio for precipitation features is 2.6, with a median aspect ratio of 2.3. Only 29% of precipitation

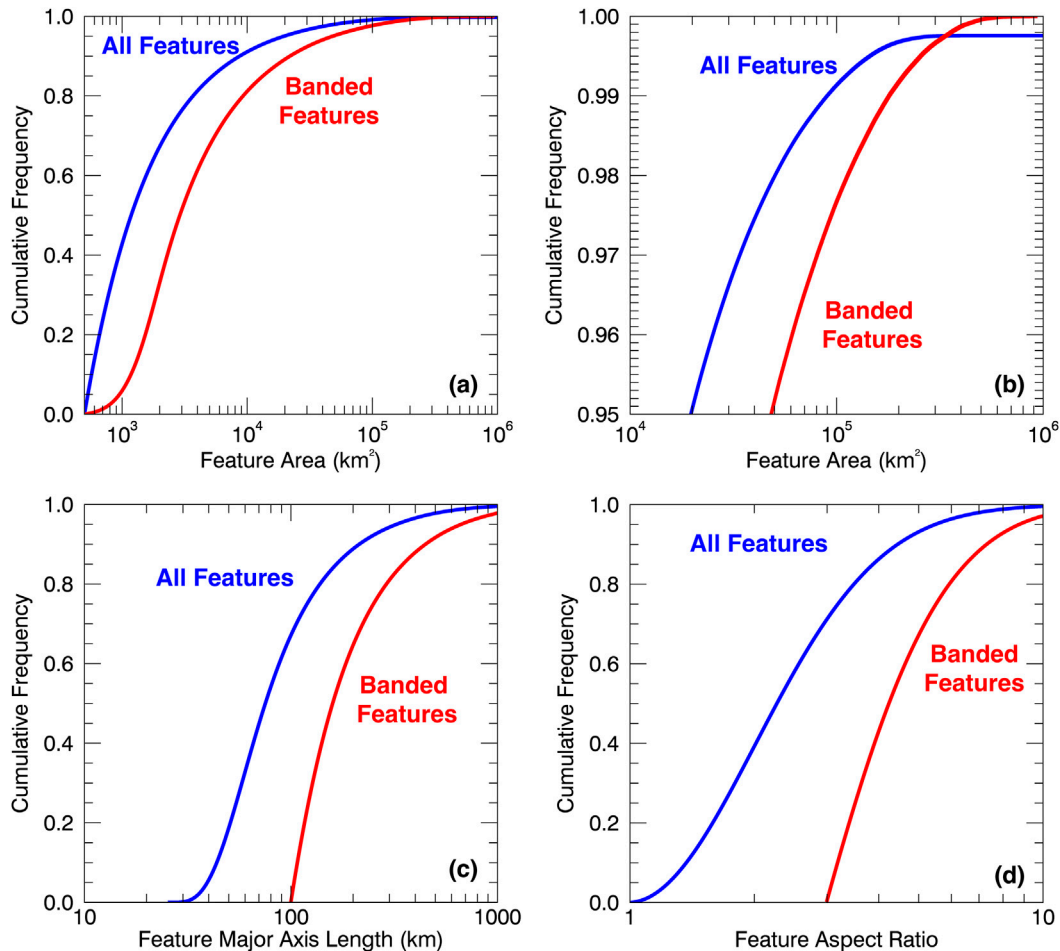


FIG. 3. (a) Cumulative frequency plot of precipitation feature area for all precipitation features (blue) and banded-precipitation features (red). (b) Cumulative frequency plot of precipitation area for all (blue) and banded (red) features from cumulative values of 0.95–1.0. (c) Cumulative frequency plot of major axis length for all (blue) and banded (red) features. (d) Cumulative frequency plot of aspect ratio for all (blue) and banded (red) features.

features have an aspect ratio greater than the 3:1 threshold for banded-precipitation features. The mean aspect ratio for banded-precipitation features is 4.9, and the median aspect ratio is 4.2. The mean values and variances of the aspect ratios from the total and banded-precipitation features are significantly different at the 99.9% level by a Student's  $t$  test and  $F$  test, respectively.

#### 4. Diurnal and annual cycles in precipitation feature shape and area

The diurnal variation in precipitation features in all seasons is shown in Fig. 4. There are two main patterns in the diurnal variation of the total precipitation area: a strong diurnal increase from  $1.7 \times 10^5$  to  $2.9 \times 10^5$  km<sup>2</sup>

from mid-May to August and relatively little diurnal variation from September to December and January to April. The mean feature area has a strong annual cycle in the diurnal pattern, with smaller summer precipitation features growing throughout the afternoon (1800–2300 UTC) (Fig. 4b), likely because of small-scale convective storms initiating during the afternoon and organizing into the evening (2300–0200 UTC). A similar pattern occurs for the major axis length (Fig. 4c). More area is covered by precipitation during the afternoon during summer than during winter and yet the average feature area is smaller; consequently, there are about 10 times more precipitating features during summer than winter (not shown). Precipitation features tend to be slightly more linear and with a weaker diurnal cycle during winter (Fig. 4d). During summer, the aspect



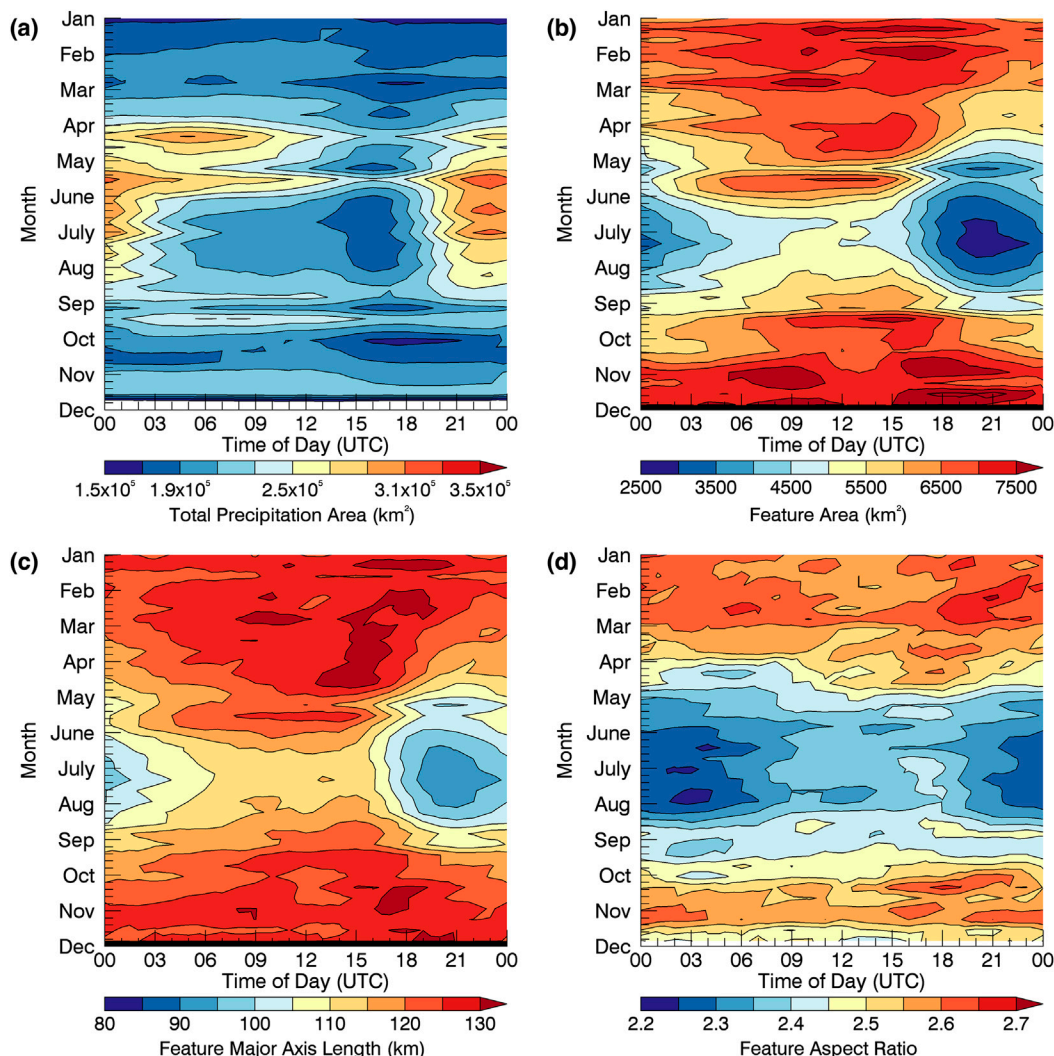


FIG. 4. Contour plots of 10-day hourly diurnal variation in (a) total area covered by all precipitation features, (b) mean precipitation feature area, (c) mean feature major axis length, and (d) mean feature aspect ratio.

ratio declines during afternoon and evening convection (Fig. 4d).

A similar set of plots, but for banded precipitation, shows that the banded-precipitation area is at its highest during the spring (Fig. 5a), potentially because of trailing cold fronts traversing the eastern United States or squall lines in the central plains. The highest amount of banded precipitation occurs during the spring, mainly from 0000 to 0900 UTC. Banded-precipitation features cover the least amount of area during summer, specifically from 1500 to 1800 UTC. The variation in mean banded-feature area is similar to the variation in the mean feature area, except that the mean banded-feature area is larger, ranging from 5000 to 17 500 km<sup>2</sup> (cf. Figs. 5b and 4b). The mean axis length for banded features (Fig. 5c) follows a similar diurnal pattern as the

major axis length for total precipitation features (cf. Figs. 5c and 4c). The mean aspect ratio of banded precipitation varies over the course of the day during the summer as the precipitation becomes more cellular during 1500–2100 UTC (Fig. 5d).

## 5. Spatial distribution of precipitation

Precipitation occurrence provides some context for judging the relative impact of banded precipitation in the climatology. In addition, by applying reflectivity thresholds for convective precipitation, the relative importance of convection in producing banded precipitation can be inferred. The number of hours per year of precipitation occurrence (Fig. 6a, herein defined as radar returns greater than or equal to 20 dBZ in the national

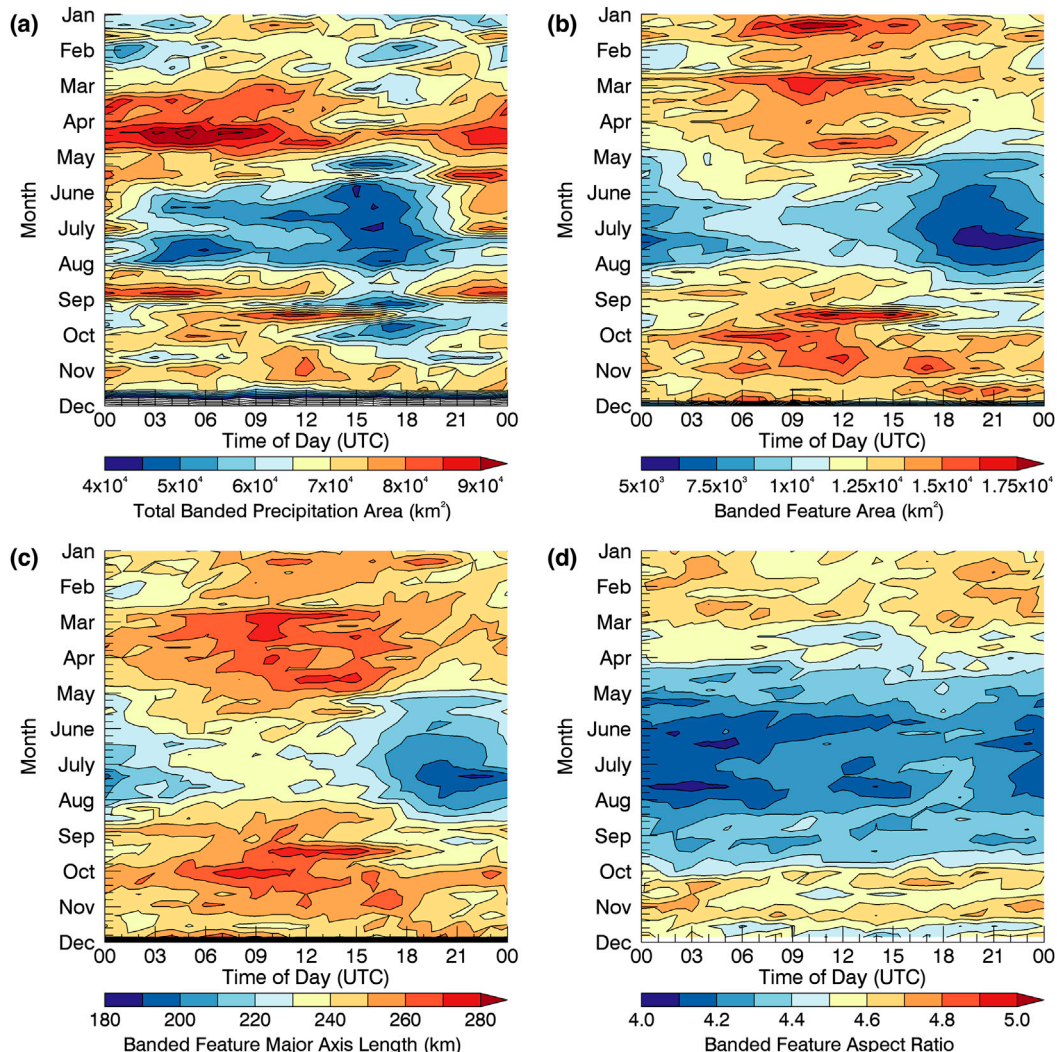


FIG. 5. Contour plots of 10-day hourly diurnal variation in (a) total area covered by banded-precipitation features, (b) mean banded-precipitation feature area, (c) mean banded feature major axis length, and (d) mean banded feature aspect ratio.

mosaic) shows a west–east gradient, with areas east of the Rockies typically having more than 300 h and areas west of the Rockies generally having fewer than 200 h. Exceptions include the northwest United States, with precipitation occurring for more than 500 h  $\text{yr}^{-1}$ , along with coastal mountain ranges in Northern California and the Sierra Nevada (Fig. 6a). East of the Mississippi River, the areas with the most frequent precipitation occur over the Ohio River valley and central Pennsylvania through New York, with a maximum over central New York to the east of Lake Ontario. The local maximum also occurs offshore of North Carolina and South Carolina as a result of the maximum in precipitation forming over the Gulf Stream (e.g., Trunk and Bosart 1990; Minobe et al. 2008). Areas of low precipitation occurrence in the

Appalachian areas of Virginia and North Carolina are most likely due to poor radar coverage caused by topographic blocking of the radar beams. Ground clutter may result in local maxima at many radar locations, particularly in the plains (Fig. 6a). When higher radar reflectivity thresholds more characteristic of deep, moist convection (e.g., 30 and 40 dBZ) are applied, the local maximum shifts southward (cf. Figs. 8a and 8b,c). Areas with the most (>60) hours per year of radar reflectivities exceeding 40 dBZ are located near the Gulf Coast, with other maxima in southeast Kansas, Tennessee, and Kentucky (Fig. 6c). These higher occurrences of higher radar reflectivities are likely due to the humid subtropical climate in the southeastern United States that supports convection year-round, as well as sea-breeze



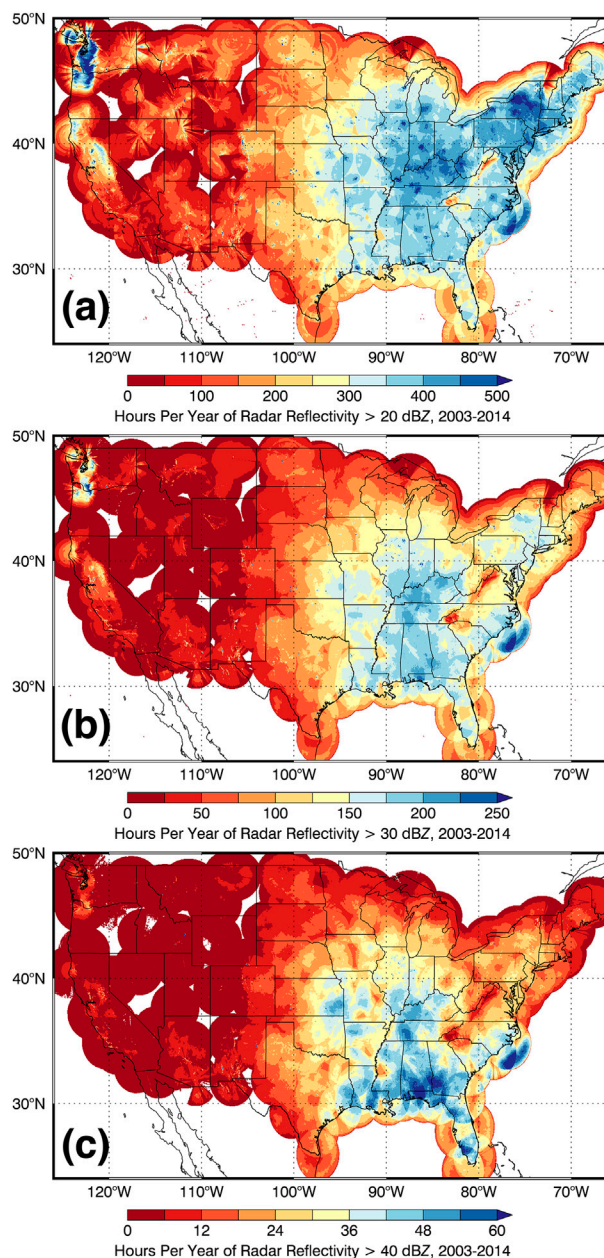


FIG. 6. Hours per year of radar reflectivity exceeding (a) 20, (b) 30, and (c) 40 dBZ.

initiation of deep convection forming hotspots along the Gulf Coast (e.g., Kirshbaum et al. 2016).

Although the annual occurrence of contiguous 20-dBZ banded-precipitation features shows a slightly different pattern than the distribution of all precipitation, a similar west–east gradient persists (cf. Figs. 6a and 7). Local maxima in banded-precipitation occurrence occur on the east sides of Lakes Michigan, Erie, and Ontario, coinciding with areas of lake-effect precipitation, and the Ohio River valley (Fig. 7), which is also the area with the

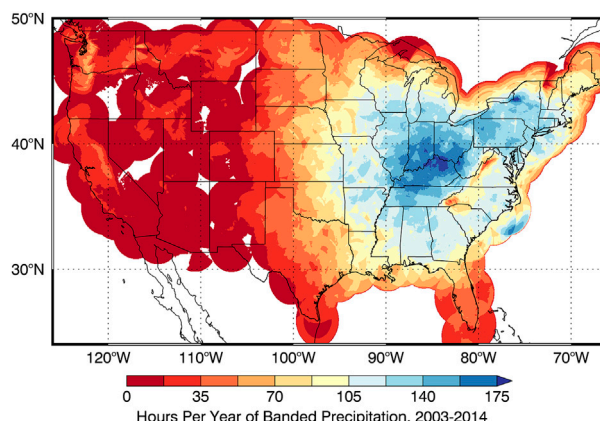


FIG. 7. Hours per year of banded-precipitation features.

maximum occurrence of precipitation (Fig. 6a). In contrast, banded-precipitation occurrence is relatively uncommon west of the Mississippi River (Fig. 7).

The percentage of banded precipitation relative to the total indicates areas where bands are relatively influential on the precipitation climatology (Fig. 8). Over most of the western United States, only 12%–16% of precipitation occurrence is from banded features. The ratio of banded to all precipitation occurrence is particularly low surrounding the radar blind spots, reflecting that the lack of radar coverage may artificially lower banded-precipitation detection. East of the Rockies, the banded percentage is fairly uniform at values greater than 32%. The locations of several radar sites are associated with low values of banded percentage as a result of nearly continuous ground clutter causing a local maximum in total precipitation occurrence. Larger areas showing a lack of coverage as seen in Fig. 8 are due to the hours of total precipitation being close to zero. As stated in section 2, over the continental United States,

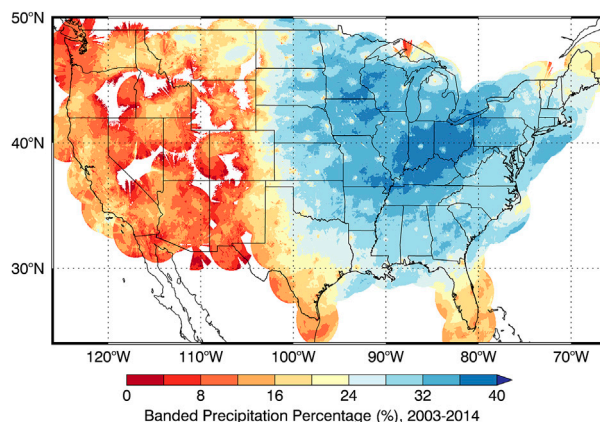


FIG. 8. Banded-precipitation percentage by hours of total precipitation.

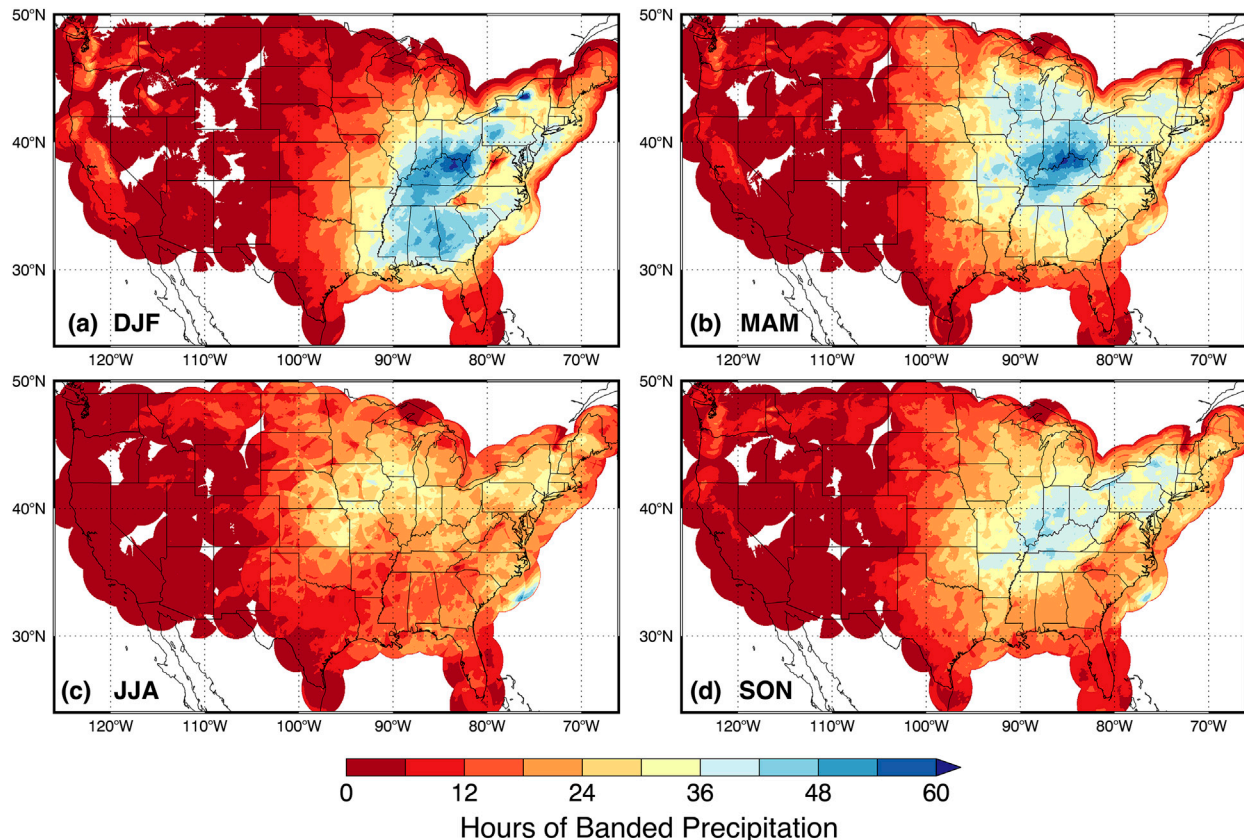


FIG. 9. Annual cycle of banded-precipitation occurrence. Annual average hours of banded-precipitation occurrence during (a) December–February (DJF), (b) March–May (MAM), (c) June–August (JJA), and (d) September–November (SON).

21.9% of precipitation by occurrence is banded. Given that only 14.8% of the precipitation features are banded, the banded features are thus generally larger than non-banded features, which is consistent with the analysis in section 3.

## 6. Annual cycle of banded precipitation

The occurrence of some types of banded-precipitation features (such as lake-effect snow and quasi-linear convective systems) varies by season and so the seasonal dependence of banded-precipitation occurrence is presented in Fig. 9. Local maxima of banding typically occur in the eastern United States during the winter (Fig. 9a). Some of these maxima shift north during spring and autumn (Figs. 9b,d). The magnitudes of the local maxima of banding are smallest in the summer, when precipitating systems tend to be more cellular (Fig. 9c). During autumn and winter, local maxima of banded precipitation occur east of Lakes Michigan, Erie, and Ontario, likely as a result of lake-effect snow (Figs. 9a,d). The maximum in the Ohio River valley is most prevalent in the winter and spring, and nonexistent in the summer (Figs. 9a–c).

A secondary maximum is present over the southeast United States during the winter (Fig. 9a). A local minimum in eastern North Carolina and Virginia extends out from the regions of poor radar coverage in the winter (Figs. 9a,b). Local maxima occur along the West Coast in winter, spring, and autumn, related to frequent frontal passages, orographic precipitation, and blocking of the radar beam by the mountains, producing spurious bands.

## 7. Regional characterization of banded precipitation

To understand the regional variability among the bands in more depth, we focus on several of the maxima in banded precipitation during January (Fig. 10a), during the season of largest banded occurrence (see Fig. 9). Local maxima occur in northern New York, western New York, northeast Ohio, and western Michigan, all positioned downwind of the Great Lakes (Fig. 10a). Banded precipitation also occurs frequently in the Ohio River valley during winter, but also during spring (Figs. 9a,b and 10a). This region is a local maximum of frontal occurrence [e.g., Fig. 1 in Berry et al. (2011)], as



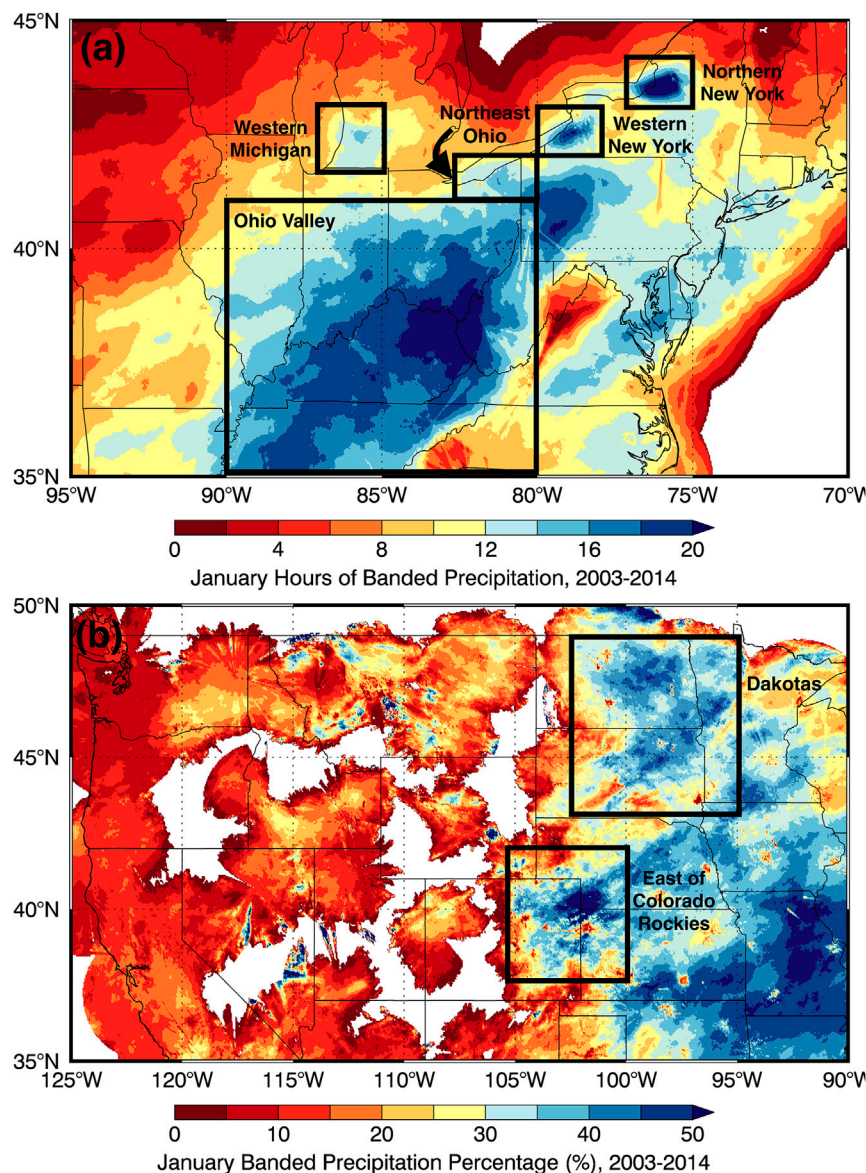


FIG. 10. (a) Hours of banded precipitation during January showing five regions of interest near the Great Lakes and the Ohio Valley. (b) Banded-precipitation percentage during January, highlighting the Dakotas and the area east of the Colorado Rockies regions of interest.

well as a frequent location for cool-season bow echoes [Fig. 2 in [Burke and Schultz \(2004\)](#)] and the climatological maximum for late-spring derechoes ([Bentley and Mote 1998, 2000](#); [Bentley and Sparks 2003](#); [Coniglio et al. 2004](#); [Coniglio and Stensrud 2004](#); [Guastini and Bosart 2016](#)).

Examining the banded percentage in January, two other maxima become apparent: eastern Colorado into Nebraska, and Kansas and the Dakotas (Fig. 11b). Indeed, previous literature has documented precipitation bands east of the Colorado Rockies (e.g., [Snook 1992](#); [Davis 1997](#); [Schumacher et al. 2010, 2015](#)) and over the Dakotas

(e.g., [Schultz and Knox 2007](#)), which are associated with the release of symmetric and inertial instabilities.

We next examine the annual cycle of precipitation and banded precipitation for the contiguous United States, as well as separately for the regions identified as the Ohio Valley, east of the Colorado Rockies, and Dakota regions (Fig. 11). Over the contiguous United States, precipitation peaks during May–July, with up to 20 h of precipitation per month on average and a weak secondary peak in December (Fig. 11a). In contrast, the occurrence of banded precipitation over the contiguous United States peaks in April and declines to a minimum

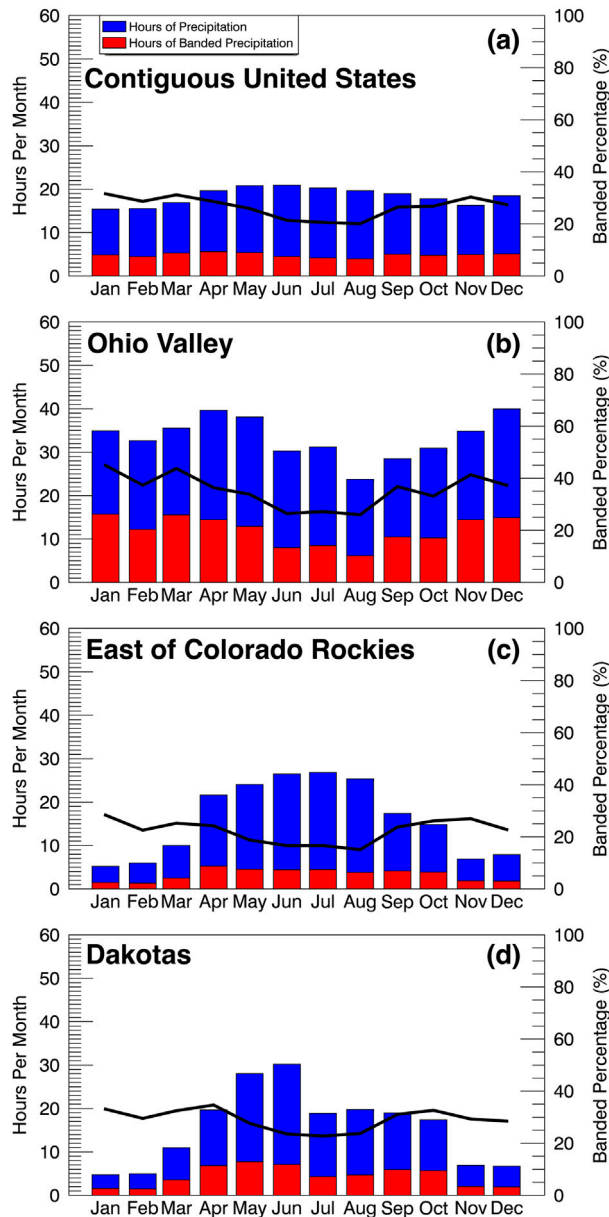


FIG. 11. Monthly average hours of all precipitation (blue) and banded precipitation (red) for (a) the contiguous United States, (b) the Ohio Valley, (c) east of the Colorado Rockies, and (d) the Dakota regions, as shown in Fig. 10. Banded percentage is shown by the black line.

during the summer (Fig. 11a), consistent with the maps of banded-precipitation occurrence (Fig. 9).

Over the Ohio Valley, precipitation peaks in April, May, and December, with up to 40 h of total precipitation (Fig. 11b). However, banded precipitation and the percentage of banded precipitation peaks during January and March (Fig. 11b). Banded precipitation over the Ohio Valley reaches a minimum during June–August.

An annual average of 400 h of precipitation occurs over the Ohio Valley, with 143 h (35.8%) of banded precipitation. The annual cycle of both total and banded precipitation over the Ohio Valley is significantly different from that of the rest of the contiguous United States, as determined by a Student's *t* test with 99.9% confidence.

The region east of the Colorado Rockies has a maximum in precipitation during the warm season with a slight decrease in banded-precipitation percentage (Fig. 11c). Only about 5 h of precipitation falls during the winter. On an annual average, 176 h of precipitation over this region east of the Colorado Rockies occurs, with 39 h (20.5%) of banded precipitation. The Dakotas possess a similar annual cycle for the region east of the Colorado Rockies (cf. Figs. 11d,c). An annual average of 187 h of precipitation occurs over this region with 52 h (28.2%) of banded precipitation. The annual cycles in total precipitation over the Dakotas and east of the Colorado Rockies and the annual cycle of banded precipitation in the Dakotas are not significantly different from that over the rest of the contiguous United States, as determined by a Student's *t* test with 99.9% confidence. In contrast, the annual cycle of banded precipitation east of the Colorado Rockies is significantly different from that over the contiguous United States with 99.9% confidence.

The lake-effect snow regions show a distinct annual cycle in both total precipitation and banded precipitation, with the maximum for both occurring during the winter months (Fig. 12). For northern New York on the east side of Lake Ontario, April, October, and December have the highest amounts of total and banded-precipitation occurrence, with an average of nearly 60 h of total precipitation and 10–12 h of banded-precipitation (Fig. 12a). The annual cycle for western New York to the east of Lake Erie peaks at a similar time of the year as that for northern New York, with more than 10 h of banded precipitation occurring during December and January and a minima of banded precipitation in the summer months (Fig. 12b). The only peaks greater than one standard deviation from the mean for banded precipitation are in December for northern New York and western New York.

Northeast Ohio exhibits a similar peak to that in both western and northern New York in banded-precipitation occurrence in December and January, but the maximum is in March after a decline in February (Fig. 12c). The decline in February, although not statistically significant, is most likely due to the freezing of the majority of western Lake Erie, compared with eastern Lakes Erie and Ontario, which are less likely to freeze (e.g., Fig. 2 in Wang et al. 2012). There is no statistically significant annual cycle for northeast Ohio, however.

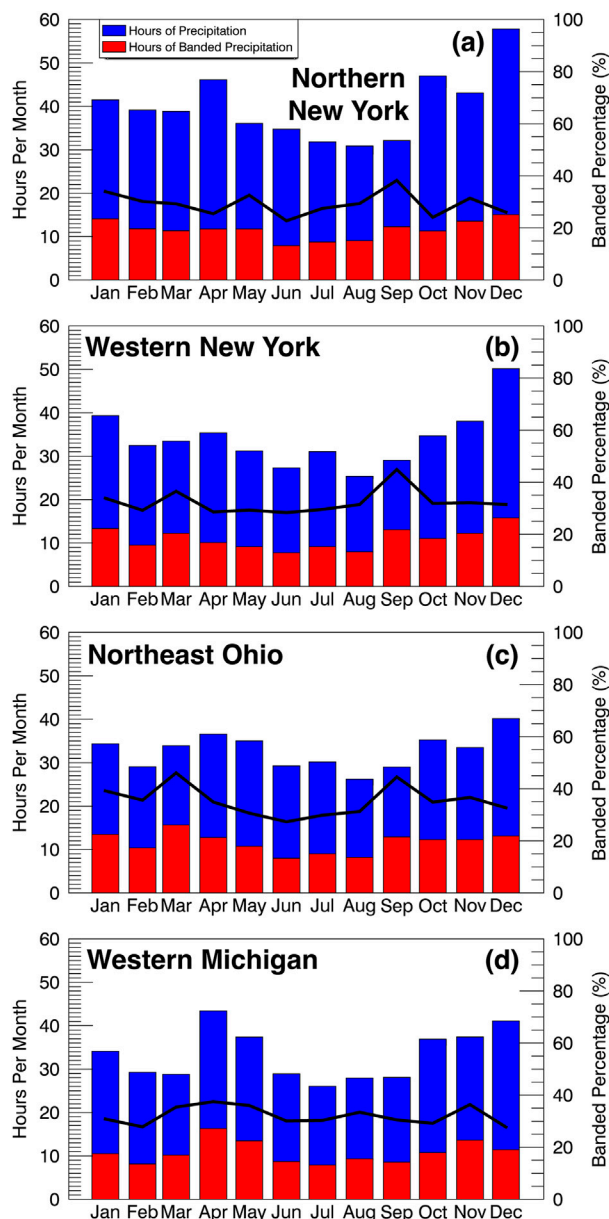


FIG. 12. Monthly average hours of all precipitation (blue) and banded-precipitation (red) occurrence for the lake-effect snow regions highlighted in Fig. 10a: (a) northern NY to the east of Lake Ontario, (b) western NY to the east of Lake Erie, (c) northeastern OH to the southeast of Lake Erie, and (d) western MI to the east of Lake Michigan. Banded percentage is shown by the black line.

Although more banded precipitation occurs in December and January than February for western Michigan (Fig. 12d), as with the other lake-effect regions, the maximum amount of banded precipitation occurs during April and May with over 8 h on average. The peak in April in western Michigan is more than one standard deviation higher than the mean. Summer corresponds to a minimum banded percentage for all regions, in agreement

with Fig. 9. Taken together, the annual average banded percentage is around 30% of all precipitation for these lake-effect regions.

The means of the annual cycles of total and banded precipitation for the lake-effect regions are all different at 95% significance as determined by a Student's *t* test and *F* test compared to the means of the contiguous United States. However, the means of the annual cycles for these four regions are not significantly different from each other. For example, the western New York and northeast Ohio regions do not pass a *t*-means test, which is unsurprising because of their mutual reliance on Lake Erie as a moisture and heat source for the lake-effect snow generation. Although there are some significant differences via *t*-means testing between different lake-effect regions (such as between northeast Ohio and northern New York), none of the regions is independent via *F*-variance tests, which is most likely due to the mutual reliance on the Great Lakes.

## 8. Caveats

In this section, we discuss three caveats to this research. First, radar coverage in the mosaic over the contiguous United States is not uniform, with gaps in coverage due to beam blocking such as over the Rocky Mountains, the Intermountain West, and the Pacific Northwest (Westrick et al. 1999; Maddox et al. 2002). As the detection of precipitation features relies on a contiguous area of radar reflectivity equal to or exceeding 20 dBZ, these gaps in coverage not only result in less occurrence of precipitation (e.g., Fig. 6), but will create artificial gaps in the detection of precipitation features. This spurious effect most likely explains the minima in banded-precipitation occurrence over the Appalachians in Virginia and North Carolina, where there is no radar coverage at 3 km above sea level (see Fig. 4a in Maddox et al. 2002). These gaps also limit the effectiveness of this analysis at determining banded-precipitation occurrence over much of the western United States.

Second, the choice of a minimum feature area of 500 km<sup>2</sup> also influences the climatology by leading to the omission of some meteorologically important bands. The bands over the Coastal Ranges of Oregon, as described in Kirshbaum and Durran (2005a,b), have average widths of about 2 km and lengths of about 20 km, which fall below the minimum size threshold in this study. This limitation, combined with the beam-blocking present in the western United States, likely underestimates band occurrence and biases band properties in these areas. Nonetheless, local maxima in banded precipitation are still apparent over the Oregon Coastal Range, Northern California, and the Sierra Nevada (Fig. 7).



Third, the choice of a mask of 20-dBZ intensity will limit the number of snowbands in our climatology because snow typically has lower radar reflectivity than rain. For example, the large snowband in Fig. 2a that stretches from Wyoming into Oklahoma is only contiguously connected by areas exceeding 5 dBZ in intensity. Similarly, a lower intensity threshold would allow more of the individual bands to be detected in the lake-effect snow case (Fig. 2e), but would result in a single contiguous feature ranging from Pennsylvania into New York instead of the four separate detected features. Despite these limitations for detecting snowbands, the method is robust enough to highlight lake-effect snow regions during winter (Figs. 9a and 10a).

## 9. Conclusions

Although the tendency for precipitation to form in bands has long been observed in both radar and satellite imagery, no previous study has quantified the occurrence of banded precipitation across the contiguous United States. This study has produced a climatology of banded precipitation by analysis of operational radar mosaics from the Iowa Environmental Mesonet every 5 min over the 12-yr period 2003–14. A banded-precipitation feature is defined as one greater than 500 km<sup>2</sup> in area, with a major axis equal to or exceeding 100 km, and an aspect ratio equal to or exceeding 3:1. An automated feature-based climatology is determined from the radar mosaics. We identify 48 916 844 precipitation features, of which 7 213 505 (14.8%) are banded. Although the vast majority of precipitation features (90%) are less than 10 000 km<sup>2</sup> in area, banded-precipitation features are generally larger with only 80% of banded-precipitation features smaller than 10 000 km<sup>2</sup>. Although banded-precipitation features account for only 14.8% of precipitation features, they contribute 21.9% to the total precipitation occurrence.

The contiguous United States exhibits a strong summer diurnal signature in total area covered by precipitation area and mean precipitation-feature area. The area covered by precipitation during July increases by a factor of 1.7 times from 1600 to 0000 UTC. This apparent signature of afternoon convection initiation and nocturnal upscale organization is not present in the winter. During winter, precipitation features are generally larger and less numerous across the contiguous United States. Wintertime precipitation also tends to be more banded. The highest total area of banded precipitation occurs during March–May, when the largest banded features also occur.

A strong west–east gradient in both precipitation occurrence and banded occurrence is present throughout this analysis. Areas west of the Rockies receive far less frequent precipitation, and these precipitation features are far less likely to be banded. Precipitation east of the

Rockies is banded around 32% of the time, whereas precipitation west of the Rockies is banded around 12%–16% of the time. Precipitation bands contribute more to the total precipitation occurrence during winter than in summer, with the total area of precipitation from banded systems peaking during spring.

Lake-effect precipitation is frequently banded, and such bands dominate the occurrence of banded precipitation east of Lakes Ontario, Erie, and Michigan. However, the area with the most consistent banded precipitation is the Ohio Valley, with an annual average of 143 h of banded precipitation, which is likely due to the prevalence of fronts and linear convective systems in this region during winter and spring. The banded-precipitation occurrence in the Ohio Valley is highest during the spring, with the highest banded percentage (>40%) occurring during January and March. In contrast, for the Dakotas and east of the Colorado Rockies, the percentage of banded precipitation is highest during winter.

This study is the first attempt to quantify all precipitation features in general, and banded precipitation specifically, over an extended period of time from the automated analysis of radar data across the contiguous United States. This method can be similarly applied to model data to verify the shape and size of precipitation features compared to observed precipitation features. Future work can use this database of precipitation features combined with meteorological parameters to determine the relative influence that prevailing winds or atmospheric conditions may have on precipitation feature size, shape, and intensity. This method can be applied to other datasets, such as the U.K. radar composite (Fairman et al. 2015), to determine the differences that may exist between the United States and the United Kingdom.

*Acknowledgments.* We thank the Iowa Environmental Mesonet for providing the radar imagery used in this article. Funding was provided by the Natural Environment Research Council (Grant NE/1024984/1) to the University of Manchester through the Precipitation Structures over Orography (PRESTO) project. The image feature detection and ellipse-fitting code was provided by the Coyote IDL Library of David Fanning (<http://www.idlcoyote.com/index.html>). We thank the three anonymous reviewers for their comments that improved this manuscript.

## REFERENCES

- Andretta, T. A., 2014: Topographic sensitivity of the Snake River Plain Convergence Zone of eastern Idaho. Part II: Numerical simulations. *Electron. J. Severe Storms Meteor.*, **9** (1). [Available online at <http://www.ejssm.org/ojs/index.php/ejssm/article/viewArticle/129>.]

- , and B. Geerts, 2010: Heavy snowfall produced by topographically induced winds in the Snake River Plain of eastern Idaho. Part I: Observational analysis. *Electron. J. Severe Storms Meteor.*, **5** (3). [Available online at <http://www.ejssm.org/ojs/index.php/ejssm/article/viewArticle/56/74>.]
- Anquetin, S., F. Miniscloux, J. D. Creutin, and S. Cosman, 2003: Numerical simulation of orographic rain. *J. Geophys. Res.*, **108**, 8386, doi:10.1029/2002JD001593.
- Barrett, A. I., S. L. Gray, D. J. Kirshbaum, N. M. Roberts, D. M. Schultz, and J. G. Fairman Jr., 2015: Synoptic versus orographic control on stationary convective banding. *Quart. J. Roy. Meteor. Soc.*, **141**, 1101–1113, doi:10.1002/qj.2409.
- , —, D. J. Kishbaum, N. M. Roberts, D. M. Schultz, and J. G. Fairman Jr., 2016: The utility of convection-permitting ensembles for the prediction of stationary convective bands. *Mon. Wea. Rev.*, **144**, 1093–1114, doi:10.1175/MWR-D-15-0148.1.
- Bentley, M. L., and T. J. Mote, 1998: A climatology of derecho-producing mesoscale convective systems in the central and eastern United States, 1986–95. Part I: Temporal and spatial distribution. *Bull. Amer. Meteor. Soc.*, **79**, 2527–2540, doi:10.1175/1520-0477(1998)079<2527:ACODPM>2.0.CO;2.
- , and —, 2000: A synoptic climatology of derecho producing mesoscale convective systems in the north-central plains. *Int. J. Climatol.*, **20**, 1329–1349, doi:10.1002/1097-0088(200009)20:11<1329::AID-JOC537>3.0.CO;2-F.
- , and J. A. Sparks, 2003: A 15 yr climatology of derecho-producing mesoscale convective systems over the central and eastern United States. *Climate Res.*, **24**, 129–139, doi:10.3354/cr024129.
- Berry, G., M. J. Reeder, and C. Jakob, 2011: A global climatology of atmospheric fronts. *Geophys. Res. Lett.*, **38**, L04809, doi:10.1029/2010GL046451.
- Burke, P. C., and D. M. Schultz, 2004: A 4-yr climatology of cold-season bow echoes over the continental United States. *Wea. Forecasting*, **19**, 1061–1074, doi:10.1175/811.1.
- Coniglio, M. C., and D. J. Stensrud, 2004: Interpreting the climatology of derechos. *Wea. Forecasting*, **19**, 595–605, doi:10.1175/1520-0434(2004)019<0595:ITCOD>2.0.CO;2.
- , —, and M. B. Richman, 2004: An observational study of derecho-producing convective systems. *Wea. Forecasting*, **19**, 320–337, doi:10.1175/1520-0434(2004)019<0320:AOSODC>2.0.CO;2.
- Cosma, S., E. Richard, and F. Miniscloux, 2002: The role of small-scale orographic features in the spatial distribution of precipitation. *Quart. J. Roy. Meteor. Soc.*, **128**, 75–92, doi:10.1256/00359000260498798.
- Davis, C. A., 1997: Mesoscale anticyclonic circulations in the lee of the central Rocky Mountains. *Mon. Wea. Rev.*, **125**, 2838–2855, doi:10.1175/1520-0493(1997)125<2838:MACITL>2.0.CO;2.
- Fairman, J. G., Jr., D. M. Schultz, D. J. Kirshbaum, S. L. Gray, and A. I. Barrett, 2015: A radar-based rainfall climatology of Great Britain and Ireland. *Weather*, **70**, 153–158, doi:10.1002/wea.2486.
- Godart, A., S. Anquetin, and E. Leblois, 2009: Rainfall regimes associated with banded convection in the Cévennes-Vivarais area. *Meteor. Atmos. Phys.*, **103**, 25–34, doi:10.1007/s00703-008-0326-3.
- Guastini, C. T., and L. F. Bosart, 2016: Analysis of a progressive derecho climatology and associated formation environments. *Mon. Wea. Rev.*, **144**, 1363–1382, doi:10.1175/MWR-D-15-0256.1.
- Hobbs, P. V., 1978: Organization and structure of clouds and precipitation on the mesoscale and microscale in cyclonic storms. *Rev. Geophys. Space Phys.*, **16**, 741–755, doi:10.1029/RG016i004p00741.
- Houze, R. A., Jr., and P. V. Hobbs, 1982: Organization and structure of precipitating cloud systems. *Advances in Geophysics*, Vol. 24, Academic Press, 225–315, doi:10.1016/S0065-2687(08)60521-X.
- , —, K. R. Biswas, and W. M. Davis, 1976: Mesoscale rainbands in extratropical cyclones. *Mon. Wea. Rev.*, **104**, 868–878, doi:10.1175/1520-0493(1976)104<0868:MRIEC>2.0.CO;2.
- Kirshbaum, D., and D. Durran, 2005a: Atmospheric factors governing banded orographic convection. *J. Atmos. Sci.*, **62**, 3758–3774, doi:10.1175/JAS3568.1.
- , and —, 2005b: Observations and modeling of banded orographic convection. *J. Atmos. Sci.*, **62**, 1463–1479, doi:10.1175/JAS3417.1.
- Kirshbaum, D. J., G. H. Bryan, R. Rotunno, and D. R. Durran, 2007a: The triggering of orographic rainbands by small-scale topography. *J. Atmos. Sci.*, **64**, 1530–1549, doi:10.1175/JAS3924.1.
- , R. Rotunno, and G. H. Bryan, 2007b: The spacing of orographic rainbands triggered by small-scale topography. *J. Atmos. Sci.*, **64**, 4222–4245, doi:10.1175/2007JAS2335.1.
- , F. Fabry, and Q. Cazenave, 2016: The Mississippi Valley convection minimum on summer afternoons: Observations and numerical simulations. *Mon. Wea. Rev.*, **144**, 263–272, doi:10.1175/MWR-D-15-0238.1.
- Liu, C., E. J. Zipser, D. J. Cecil, S. W. Nesbitt, and S. Sherwood, 2008: A cloud and precipitation feature database from nine years of TRMM observations. *J. Appl. Meteor. Climatol.*, **47**, 2712–2728, doi:10.1175/2008JAMC1890.1.
- Maddox, R. A., J. Zhang, J. J. Gourley, and K. W. Howard, 2002: Weather radar coverage over the contiguous United States. *Wea. Forecasting*, **17**, 927–934, doi:10.1175/1520-0434(2002)017<0927:WRCOTC>2.0.CO;2.
- Mass, C. F., 1981: Topographically forced convergence in western Washington State. *Mon. Wea. Rev.*, **109**, 1335–1347, doi:10.1175/1520-0493(1981)109<1335:TFCIWW>2.0.CO;2.
- Miner, T. J., and J. M. Fritsch, 1997: Lake-effect rain events. *Mon. Wea. Rev.*, **125**, 3231–3248, doi:10.1175/1520-0493(1997)125<3231:LERE>2.0.CO;2.
- Miniscloux, F., J. D. Creutin, and S. Anquetin, 2001: Geostatistical analysis of orographic rainbands. *J. Appl. Meteor.*, **40**, 1835–1854, doi:10.1175/1520-0450(2001)040<1835:GAOOR>2.0.CO;2.
- Minobe, S., A. Kuwano-Yoshida, N. Komori, S.-P. Xie, and R. J. Small, 2008: Influence of the Gulf Stream on the troposphere. *Nature*, **452**, 206–209, doi:10.1038/nature06690.
- Nesbitt, S. W., E. J. Zipser, and D. J. Cecil, 2000: A census of precipitation features in the tropics using TRMM: Radar, ice scattering, and lightning observations. *J. Climate*, **13**, 4087–4016, doi:10.1175/1520-0442(2000)013<4087:ACOPFI>2.0.CO;2.
- , R. Cifelli, and S. A. Rutledge, 2006: Storm morphology and rainfall characteristics of TRMM precipitation features. *Mon. Wea. Rev.*, **134**, 2702–2721, doi:10.1175/MWR3200.1.
- Niziol, T. A., W. R. Snyder, and J. S. Waldstreicher, 1995: Winter weather forecasting throughout the eastern United States. Part IV: Lake effect snow. *Wea. Forecasting*, **10**, 61–77, doi:10.1175/1520-0434(1995)010<0061:WWFTTE>2.0.CO;2.
- Norris, J., G. Vaughan, and D. M. Schultz, 2013: Snowbands over the English Channel and Irish Sea during cold-air outbreaks. *Quart. J. Roy. Meteor. Soc.*, **139**, 1747–1761, doi:10.1002/qj.2079.
- , —, and —, 2014: Precipitation banding in idealized baroclinic waves. *Mon. Wea. Rev.*, **142**, 3081–3099, doi:10.1175/MWR-D-13-00343.1.
- Novak, D. R., L. F. Bosart, D. Keyser, and J. S. Waldstreicher, 2004: An observational study of cold season banded precipitation in northeast U.S. cyclones. *Wea. Forecasting*, **19**, 993–1010, doi:10.1175/815.1.

- , J. S. Waldstreicher, D. Keyser, and L. F. Bosart, 2006: A forecast strategy for anticipating cold season mesoscale band formation within eastern U.S. cyclones. *Wea. Forecasting*, **21**, 3–23, doi:[10.1175/WAF907.1](https://doi.org/10.1175/WAF907.1).
- , B. A. Colle, and A. R. Aiyyer, 2009: Evolution of mesoscale precipitation band environments within the comma head of northeast U.S. cyclones. *Mon. Wea. Rev.*, **137**, 2662–2686, doi:[10.1175/2009MWR2874.1](https://doi.org/10.1175/2009MWR2874.1).
- Parsons, D. B., and P. V. Hobbs, 1983: The mesoscale and microscale structure and organization of clouds and precipitation in mid-latitude cyclones. XI: Comparisons between observational and theoretical aspects of rainbands. *J. Atmos. Sci.*, **40**, 2377–2398, doi:[10.1175/1520-0469\(1983\)040<2377:TMAMSA>2.0.CO;2](https://doi.org/10.1175/1520-0469(1983)040<2377:TMAMSA>2.0.CO;2).
- Rauber, R. M., and Coauthors, 2014: Stability and charging characteristics of the comma head region of continental winter cyclones. *J. Atmos. Sci.*, **71**, 1559–1582, doi:[10.1175/JAS-D-13-0253.1](https://doi.org/10.1175/JAS-D-13-0253.1).
- Schmit, T. J., and Coauthors, 2015: Rapid refresh information of significant events: Preparing users for the next generation of geostationary operational satellites. *Bull. Amer. Meteor. Soc.*, **96**, 561–576, doi:[10.1175/BAMS-D-13-00210.1](https://doi.org/10.1175/BAMS-D-13-00210.1).
- Schultz, D. M., and J. A. Knox, 2007: Banded convection caused by frontogenesis in a conditionally, symmetrically, and inertially unstable environment. *Mon. Wea. Rev.*, **135**, 2095–2110, doi:[10.1175/MWR3400.1](https://doi.org/10.1175/MWR3400.1).
- , D. S. Arndt, D. J. Stensrud, and J. W. Hanna, 2004: Snowbands during the cold-air outbreak of 23 January 2003. *Mon. Wea. Rev.*, **132**, 827–842, doi:[10.1175/1520-0493\(2004\)132<0827:SDTCOO>2.0.CO;2](https://doi.org/10.1175/1520-0493(2004)132<0827:SDTCOO>2.0.CO;2).
- Schumacher, R. S., D. M. Schultz, and J. A. Knox, 2010: Convective snowbands downstream of the Rocky Mountains in an environment with conditional, dry symmetric, and inertial instabilities. *Mon. Wea. Rev.*, **138**, 4416–4438, doi:[10.1175/2010MWR3334.1](https://doi.org/10.1175/2010MWR3334.1).
- , —, and —, 2015: Influence of terrain resolution on banded convection in the lee of the Rocky Mountains. *Mon. Wea. Rev.*, **143**, 1399–1416, doi:[10.1175/MWR-D-14-00255.1](https://doi.org/10.1175/MWR-D-14-00255.1).
- Smalley, M., and T. L'Ecuyer, 2015: A global assessment of the spatial distribution of precipitation occurrence. *J. Appl. Meteor. Climatol.*, **54**, 2179–2197, doi:[10.1175/JAMC-D-15-0019.1](https://doi.org/10.1175/JAMC-D-15-0019.1).
- Snook, J. S., 1992: Current techniques for real-time evaluation of conditional symmetric instability. *Wea. Forecasting*, **7**, 430–439, doi:[10.1175/1520-0434\(1992\)007<0430:CTFRTE>2.0.CO;2](https://doi.org/10.1175/1520-0434(1992)007<0430:CTFRTE>2.0.CO;2).
- Trunk, T. J., and L. F. Bosart, 1990: Mean radar echo characteristics during Project GALE. *Mon. Wea. Rev.*, **118**, 459–469, doi:[10.1175/1520-0493\(1990\)118<0459:MRECDP>2.0.CO;2](https://doi.org/10.1175/1520-0493(1990)118<0459:MRECDP>2.0.CO;2).
- Wang, J., X. Bai, H. Hu, A. Clites, M. Colton, and B. Lofgren, 2012: Temporal and spatial variability of Great Lakes ice cover, 1973–2010. *J. Climate*, **25**, 1318–1329, doi:[10.1175/2011JCLI4066.1](https://doi.org/10.1175/2011JCLI4066.1).
- Westrick, K. J., C. F. Mass, and B. A. Colle, 1999: The limitations of the WSR-88D radar network for quantitative precipitation measurement over the coastal western United States. *Bull. Amer. Meteor. Soc.*, **80**, 2289–2298, doi:[10.1175/1520-0477\(1999\)080<2289:TLOTWR>2.0.CO;2](https://doi.org/10.1175/1520-0477(1999)080<2289:TLOTWR>2.0.CO;2).
- Xu, W., S. A. Rutledge, C. Schumacher, and M. Katsuma, 2015: Evolution, properties, and spatial variability of MJO convection near and off the equator during DYNAMO. *J. Atmos. Sci.*, **72**, 4126–4147, doi:[10.1175/JAS-D-15-0032.1](https://doi.org/10.1175/JAS-D-15-0032.1).
- Yamada, T. J., J. Sasaki, and N. Matsuoka, 2012: Climatology of line-shaped rainbands over northern Japan in boreal summer between 1990 and 2010. *Atmos. Sci. Lett.*, **13**, 133–138, doi:[10.1002/asl.373](https://doi.org/10.1002/asl.373).